Biomass Conversion and Biorefinery
https://doi.org/10.1007/s13399-023-04575-1

ORIGINAL ARTICLE

Co-pyrolysis behavior of polylactic acid and biomass from heated tobacco products

Miao Liang[1] · Haiyang Pan[1] · Yuanyang Zhu[2] · Haibo Zhu[2] · Man Su[2] · Yifei Xie[2] · Yongjie Zheng[2] · Xi Jiang[1] · Ruili Li[1] · Junsong Zhang[1]

Received: 3 May 2023 / Revised: 23 June 2023 / Accepted: 29 June 2023

Abstract

In this study, the co-pyrolysis behavior of waste tobacco (WT) and polylactic acid (PLA) from heated tobacco products (HTPs) was investigated by TG, TG-FTIR, and Py-GC/MS in order to reveal the synergistic mechanism during the co-pyrolysis process from the perspective of pyrolytic kinetic parameters and product distribution. The addition of WT during the pyrolysis of PLA reduced the T_{max} from 367.5 to 303.8−314.1°C, indicating a notable synergistic effect between PLA and WT during the co-pyrolysis process. Pyrolysis kinetic analysis also indicated the enhanced thermal activity of PLA as reflected by the reduced activation energy, especially when the proportion of WT was wt. 25%, the activation energy was reduced from 166.38 to 111.20 KJ/mol. Meanwhile, the decreased ΔG for the co-pyrolysis of PLA/WT may also indicate an enhanced reaction reactivity. The pyrolytic products detected by TG-FTIR showed that the addition of WT-promoted free radical reactions during the co-pyrolysis process as reflected by the reduction of CO and aldehyde. Py-GC/MS results indicated that for PLA/WT= 1:1, the yield of lactide increased threefold, indicating a significant synergistic effect. In summary, the co-pyrolysis of PLA and WT could effectively tap into residual value from discarded HTPs in resource recovery field and solve potential environmental pollution problems.

Keywords Heated tobacco products · Co-pyrolysis · Synergistic effects · Polylactic acid

1 Introduction

Heated tobacco products (HTPs) were a newly emerging tobacco product that utilized a controlled external heat source to maintain a specific temperature for smoldering the tobacco materials [1]. In this manner, the smoking that contained nicotine, glycerol, and flavoring substances can be generated under a heating but not a burning condition. Reports has shown that the smoke released from HTPs exhibited a significantly reduced combustion-derived toxicants due to the special heating temperature as compared with traditional cigarettes [2]. Generally, HTPs contains

✉ Haibo Zhu
nt_zhuhb@jszygs.com

✉ Junsong Zhang
13283712413@163.com

Miao Liang
liangmiaozzu@163.com

Haiyang Pan
13027624926@163.com

Yuanyang Zhu
zhuyuanyang202304@163.com

Man Su
suman202304@163.com

Yifei Xie
xyifei202304@163.com

Yongjie Zheng
zzuli505baobao@163.com

Xi Jiang
15238020298@163.com

Ruili Li
17633759047@163.com

[1] Collaborative Innovation Center of Food Production and Safety, College of Food and Bioengineering, Zhengzhou University of Light Industry, Zhengzhou 450001, P. R. China

[2] Research and Development Center, Nantong Cigarette Filter Co., Ltd., Nantong 226000, P. R. China

Published online: 18 July 2023

three components: a tobacco materials part that rolled from reconstituted tobacco and treated with humectant, an acetate fiber filter rod and a polylactic acid (PLA) polymer film [3].

Among of these three parts, the tobacco materials part was mainly used for the generation of nicotine and various flavor substances to satisfy the needs of consumers [4]. The PLA film was a special component that distinguishes HTPs from traditional cigarettes. The function of PLA was used to reduce the temperature of mainstream smoke during HTPs inhalation by phase change heat absorption, simulating the inhalation experience of traditional cigarettes. At the same time, PLA could also adsorb harmful substances in the smoke aerosol to a certain extent [5]. Nowadays, as consumer health awareness increases, the consumption of HTPs increased significantly. Therefore, a large amount of waste HTPs was produced and dumped into the environment without appropriate treatment, which caused potential environmental pollution and waste of bioresources [6]. It is highly desirable to the reasonable utilization of these discarded resources from HTPs [7].

Pyrolysis technique was a promising method for the conversion of these waste resources into value-added bio-oil, pyrolytic gas and carbon materials [8–10]. Several studies have focused on the pyrolysis behavior of PLA or WT. For the PLA, Chien et al [11]. used on-line thermogravimetry-mass spectrometry (TG-MS) to determine the polycyclic aromatic hydrocarbons (PAHs) content released from PLA pyrolysis, and found that the total PAH emissions for PLA pyrolysis was significantly lower than the values associated with PLA combustion. Zhang et al. [12] used thermogravimetric fourier infrared spectroscopy/gas chromatography−mass spectrometry (TG- FTIR/GC-MS) to analyze the pyrolysis characteristic of 3D printed poly lactic acid waste (3DP-PLAW). They found that the high volatile matter content of 3DP- PLAW resulted in a more efficient thermochemical conversion. As for the pyrolysis of WT, Zeynep et al. [13] used FT-IR (Fourier transform infrared spectroscopy), GC-MS, and PMR (proton magnetic resonance) techniques to characterize the bio-oil obtained from the pyrolysis of tobacco waste in a fixed-bed reactor. The results showed that the bio-oil consists mainly of nicotine (26.78%), phenol (8.02%), and limonene (4.59%) compounds. Xia et al. [14] investigated the production of aroma compounds from the fast pyrolysis of two kinds of tobacco waste, that was tobacco leaf fragments (TF) and tobacco stems (TS) in a fluidized bed pyrolysis reactor. The results indicated that when TF was used as raw materials, low-temperature (about 350 °C) pyrolysis was beneficial for the production of aroma compounds, whereas TS required higher temperature (more than 380 °C) to reach the optimal pyrolysis process. The above studies were only focused on the pyrolysis process of individual waste material, nevertheless the co-pyrolysis behavior of PLA and WT was seldom studied.

The pyrolysis process of PLA under inert gas includes both transesterification reaction and free radical reaction at low and high temperatures, respectively [15]. At lower temperatures, the carboxyl or hydroxyl groups on the PLA molecule chain are reversed to form acetaldehyde, carbon monoxide, lactides (L-lactide and D-lactide), and cyclic polymers similar to lactides [16]. When the pyrolysis temperature reaches to 270- 280 °C, PLA mainly undergoes a free radical reaction [17] as shown in Fig. 1. Actually, the co-pyrolysis of PLA with biomass was an important and efficient strategy for the production of specific valuable pyrolysis products due to the synergistic effect, which could facilitate the pyrolysis reaction and reduce the energy required for the pyrolysis [18]. For instance, Sun et al. [19] studied the co-pyrolysis behavior of PLA and the major components of biomass (cellulose, hemicellulose and lignin). It was found that the pyrolysis of lignin provided additional free radicals and reduced the activation energy of PLA. Waste PLA and tobacco biomass were the main components of HTPs, and there were considerable amount of lignin was existed in the tobacco biomass after the consumption of HTPs. This provided clue for the investigation of co-pyrolysis behavior of PLA and WT.

Therefore, the co-pyrolysis of WT and PLA was studied by using thermogravimetry, TG-FTIR and Py-GC/MS. DAEM (Distributed Activation Energy Model), FWO (Flynn-Wall-Ozawa), and Starink methods based on the thermogravimetric data were used to determine and compare the pyrolysis kinetic parameters of the samples. Furthermore, the gaseous products during the co-pyrolysis process was analyzed through TG-FTIR, Py-GC/MS and self-built tubular furnace pyrolysis experiment. This study may be beneficial for the rational utilization of HTPs waste in the thermochemical conversion manner.

2 Materials and methods

2.1 Materials and sample preparation

HTPs was provided by Inner Mongolia Kunming Cigarette Co. Ltd. After the products were smoked, WT and PLA were removed from the HTPs by grinding and screening to obtain particles with particle size less than 500 μm. In addition, the PLA and WT were blended in the mass proportion of 1:3, 1:1, and 3:1 in order to investigate the interaction during co-pyrolysis process. The samples were dried in oven under 80 °C for 48 h before the experiments.

The elemental composition of the samples was determined using an elemental analyzer (Vario EL cube; Germany). The percentage contents of C, H, and O were 45.41%, 5.83%, and 45.59% for WT and 49.60%, 5.09%, and 44.26% for PLA, respectively.

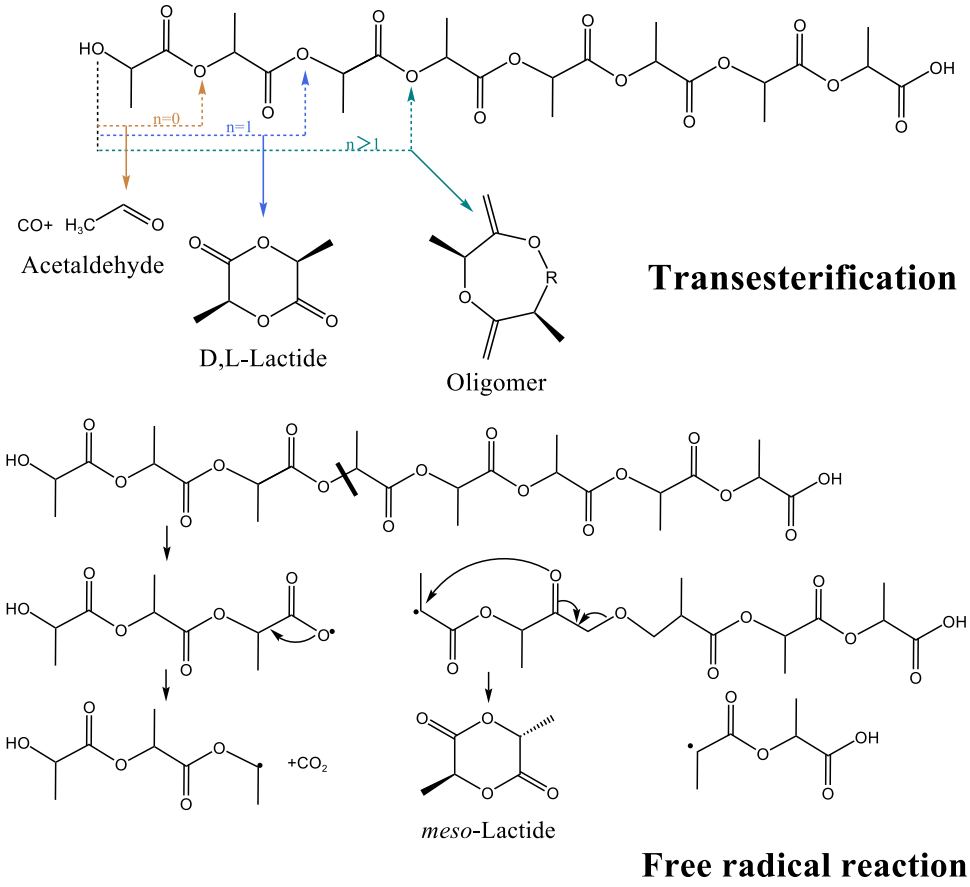

Fig. 1 The pyrolysis mechanism of transesterification and radical reaction of PLA

2.2 Thermogravimetric analysis

Thermogravimetric analysis of PLA, WT, and PLA/WT blends was performed using a thermogravimetric analyzer (Discovery, TA, USA). For each experiment, approximately 20 mg of the sample was loaded into the platinum crucible under the nitrogen atmosphere at a flow rate of 50 mL/min. The feedstock was heated from 40 to 800 °C under different heating rates of 10, 20, and 40 °C/min, respectively. The characteristic parameters such as the maximum pyrolysis rate (DTG_{max}) and its corresponding temperature (T_{max}) were determined from thermogravimetry (TG) and derivative thermogravimetry (DTG) (first-order derivative of TG) curves according to the method reported in previous studies [20].

2.3 Kinetic analysis

Generally, model-fitting method like iso-conversional method are the available techniques to determine the kinetic parameters of the reaction for understanding the thermal conversion process undergoing during pyrolysis [21]. During the pyrolysis of solid materials, the decomposition rate follows the formula [22]; and k(T) is the reaction rate constant given by Arrhenius equation:

$$\frac{d\alpha}{dt} = k(T)f(\alpha) \tag{1}$$

$$\mathrm{k(T)} = \mathrm{Aexp}\left(-\frac{E_a}{RT}\right) \tag{2}$$

where A and E_a are the pre-exponential factor (min^{-1}) and activation energy (kJ/mol) of the pyrolysis reaction, respectively; R is the universal gas constant of 8.314 J/K mol and T is the absolute temperature (K). dα/dt refers to the decomposition rate. α refers to conversion degree which can be expressed as:

$$\alpha = \frac{m_0 - m_t}{m_0 - m_\infty} \tag{3}$$

where m_0 was the initial samples mass; m_t was the final samples mass; m_∞ was the mass of samples at time t. In TG analysis, the constant heating rate (β) can be expressed as β = dT/dt. The pyrolysis rate can be expressed as:

$$\frac{d_\alpha}{d_t} = \frac{A}{\beta}\exp\left(-\frac{E_\alpha}{RT}\right)f(\alpha) \tag{4}$$

Three model-free methods, that is Flynn-Wall-Ozawa (FWO), distributed activation energy model (DAEM),

Starink, were chosen to study kinetic analysis of the pyrolysis of PLA and WT/PLA. There is no need to select reaction mechanism using these three model-free methods, so that the errors of E_a estimate can be avoided [23]. The three model-free methods are respectively [16, 24]:

$$\mathrm{FWO}: \lg(\beta) = \lg\left(\frac{AE_a}{Rg(\alpha)}\right) - 2.315 - 0.4567\frac{E_a}{RT} \quad (5)$$

$$\mathrm{DAEM}: \ln\left(\frac{\beta}{T^2}\right) = \ln\left(\frac{AR}{E_a}\right) + 0.6575 - \frac{E_a}{RT} \quad (6)$$

$$\mathrm{Starink}: \ln\left(\frac{\beta}{T^{1.92}}\right) = C_S - 1.008\frac{E_a}{RT} \quad (7)$$

There is linear relationship between 1/T and lgβ (FWO), $\ln[\beta/T^2]$(DEAM), and $\ln[\beta/T^{1.92}]$ (Starink) at different heating rates. The activation energy E_a can be calculated from the linear plots for each conversion degree.

The thermochemical parameters including enthalpies (ΔH) and Gibbs free energies (ΔG) can be calculated by Eqs. (8)– (12) [17]:

$$\mathrm{A} = \left(\beta \bullet \mathrm{E_a} \bullet \exp\left(\frac{\mathrm{E_a}}{\mathrm{RT_m}}\right)\right)/\left(\mathrm{RT_m^2}\right) \quad (8)$$

$$\mathrm{G}(\alpha) = \int_0^{\alpha}\frac{\mathrm{d}_\alpha}{1-\alpha} = \int_0^{\mathrm{T}}\frac{\mathrm{A}}{\beta}\exp\left(-\frac{\mathrm{E}_\alpha}{\mathrm{RT}}\right)\mathrm{dT} \quad (9)$$

$$\Delta\mathrm{H} = E_a - RT \quad (10)$$

$$\Delta\mathrm{G} = \mathrm{E_a} + \mathrm{RT_m}\ln\left(\frac{\mathrm{K_B T_m}}{\mathrm{hA}}\right) \quad (11)$$

$$\Delta\mathrm{S} = (\Delta\mathrm{H} - \Delta\mathrm{G})/\mathrm{T_m} \quad (12)$$

where K_B (1.381×10^{-23} J/K) is the Boltzmann constant, h (6.626×10^{-34} J/S) is the Planck constant, and T_m (K) is peak temperature of the DTG curve.

2.4 TG-FTIR analysis

The release behavior of gaseous products during the pyrolysis process of samples were monitored by a TG instrument (NETZSCH TG 209F3) coupled with an FTIR spectrometer (Nicolet 8700; Thermo Electron, America). The loading amount of samples and furnace atmosphere were consistent with the above TG experiment under the heating rate of 20 °C/min. The released volatiles during the pyrolysis process were analyzed online using the FTIR spectrometer recorded from 400 to 4000 cm^{-1} at a resolution of 2 cm^{-1}. The transfer line used to connect TG and FTIR was heated to 230 °C to prevent the condensation of gaseous products.

2.5 Py-GC/MS analysis

A pyrolyzer (Py) (CDS5200, Agilent, USA) combined with gas chromatography (GC)/mass spectroscopy (MS) (Agilent 6890N/Agilent 5973i, Agilent, USA) was used to investigate the chemical distribution of products obtained from the pyrolysis of PLA, WT, and PLA/WT blends at 600 °C. A 1 mg sample in a deactivated metal cup was introduced to the preheated furnace of the pyrolyzer. The pyrolysis product emitted by the pyrolyzer was transferred to a GC capillary column (UA-5, 30 m × 0.25 mm i.d. × 0.25 µm ft) via a split/split less GC inlet (300 °C, split ratio: 100/1) and cryo-focused with liquid nitrogen at the front point of the column. After cryo-focusing, the pyrolysis products were separated in the column under non-isothermal GC oven heat condition, from 40 °C (3-min hold) to 280 °C (3-min hold) at 20 °C / min and detected by MS in scan mode (m/z, 40–500). All peaks monitored on total ion chromatogram were identified using an MS library (NIST 14) and integrated to compare their amounts indirectly using absolute peak areas. The average MS peak areas for all pyrolysis products, which were obtained through repeated Py-GC/MS analysis, were used as the amounts of pyrolysis products.

2.6 Infrared heated tubular furnace combined with GC/MS analysis

The pyrolysis experiment of PLA, WT, and their blends was further conducted on the self-built infrared-heated tubular furnace [25]. The sample of 0.4 g was heated to 600 °C and maintained for 5 min at a heating rate of 20 °C/s. The tubular furnace was continuously flushed with N_2 under a flow rate of 200 mL/min to ensure an inert atmosphere. The pyrolytic produces generated was captured through a Cambridge filter held by the holder.

The pyrolytic products collected by the filter were extracted by dichloromethane and analyzed by using a 8890-5977B GC/MS analyzer (Agilent, USA) coupled with a HP-5 capillary column (60 m long, 0.25-mm diameter with a film thickness of 0.25 µm). The carrier gas was high-purity helium, and its flow rate was set at 1.0 mL/min. The temperature program of column oven was set as follows: at a constant temperature of 40 °C for 5 min, 40–250 °C at a rate of 3 °C/min, followed by 250–280 °C at a rate of 20 °C/min, and remained at this temperature for 5 min. The mass spectrometer was operated under the electron impact (EI) mode with electron energy at 70 eV and scanning range of 35–550 m/z in the full scan mode method. The quadrupole temperature, ion source temperature, and the transfer line temperature were 150 °C, 230 °C, and 280 °C,

respectively. A specific concentration of phenylethyl acetate-dichloromethane compound was used as internal standard for quantification. The products were identified by matching against the NIST database.

3 Results and discussion

3.1 Thermogravimetric analyses

The TG and DTG curves of WT, PLA, and PLA/WT blends at a heating rate of 10 °C/min were shown in Fig. 2. It could be seen from the figure that the main pyrolysis region of PLA was 295¯396 °C, with the maximum weight loss rate temperature of 366 °C and residual ash content of 1.19%. The DTG_{max} of PLA was 35.69 %/min which was relatively higher than that of other samples. The narrow thermal degradation temperature range of PLA indicated that this material has completely undergone thermal degradation due to its ordered PLA molecular chains structure with high similarity [26]. The pyrolysis of WT could be divided into four stages as shown by the DTG curve. These stages consisted of dehydration (stage I, 30–94.7 °C), decomposition of volatile components and hemicellulose (stage II, 94.7–219.4 °C), decomposition of cellulose and lignin (stage III, 219.4–549.9 °C), and decomposition of inorganic salts (stage IV, 549.9–800.0 °C) [27]. The first stage occurred at 30–94.7 °C. In the first stage, the free water and bound water in the WT was released slowly [28]. The second and third stage was classified as 94.7−549.9 °C, with the maximum rate of weight loss occurring at 314 .8 °C. This stage was mainly attributed to the further degradation of monosaccharides, oligosaccharides, small organic acids, free amino acids, and other heat destabilized volatile components and the pyrolysis of biomass compounds such as glycerol, proteins, lipid-like macromolecules and hemicellulose, cellulose, and lignin in WT [29]. Due to the low-temperature baking at around 300 °C, a large amount of volatiles were lost and hemicellulose and cellulose were significantly reduced in WT, which led to the lignin dominating the pyrolysis of WT and thus making its pyrolysis reaction more gentle.

In order to better characterize the effect of synergistic effects on PLA pyrolysis properties in the co-pyrolysis of PLA and WT, experimental results and theoretical TG/DTG curves of PLA/WT blends with different ratios were compared. The theoretical mass loss of PLA/WT blends can be expressed as [30]:

$$W_{blend} = \omega_{WF} * W_{WT} + \omega_{PLA} * W_{PLA} \quad (13)$$

In the formula, W_{blend} is the theoretical mass loss of PLA/WT blend, ω is the mass percentage of PLA or WT in the blend and W is the mass loss of either solo PLA or WT. The theoretical TG and DTG curves of PLA/WT thermal degradation process were obtained by calculation and plotted as shown in Fig. 3, which were compared with experimental TG and DTG curves.

As can be seen from Fig. 3 and Table 1, the T_{max} for PLA was 367.5 °C. In the three different ratios of PLA/WT blends, the T_{max} was lower than that of solo PLA. With the increase of WT in the blends, the T_{max} decreased from 314.1 to 303.8 °C. This indicated that the addition of WT could decreased the pyrolysis temperature interval of PLA, which allowed PLA to pyrolyze at a lower temperature. Meanwhile, there was no significant difference between the residual mass from the experimental TG and theoretical TG curves at temperature of 800 °C. This indicated that the effect of WT addition on the residue carbon was not obvious. As for the PLA/WT=1:3 sample, the experimental weight loss increased by 4.28% compared with the theoretical value, and the experimental DTG_{max} increased by 2.63% compared with the theoretical value. As for the PLA/WT=1:1 sample, the experimental weight loss of the sample increased by 9.31%, and the experimental DTG_{max} increased by 8.10 %/min, indicating that the co-pyrolysis could improve the pyrolysis yield of PLA and intensify the reaction. As for the PLA/WT=3:1 sample, although the pyrolysis interval was shifted to lower temperature, there was no obvious increase

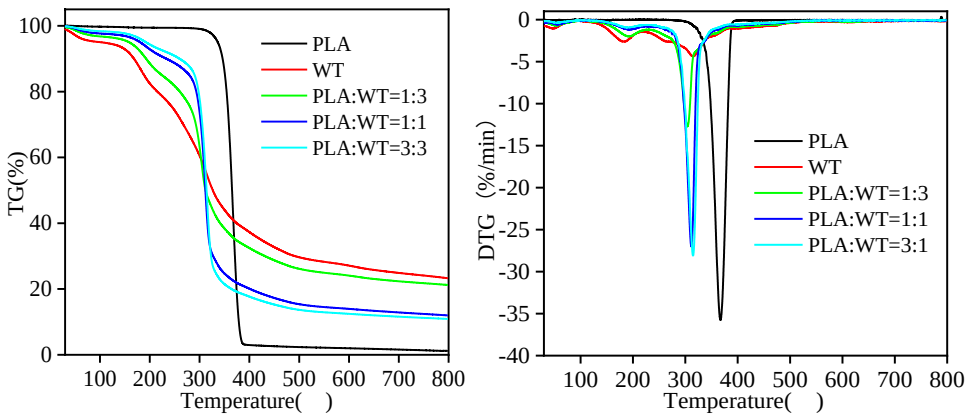

Fig. 2 The TG and DTG curves of WT, PLA and PLA/WT blends

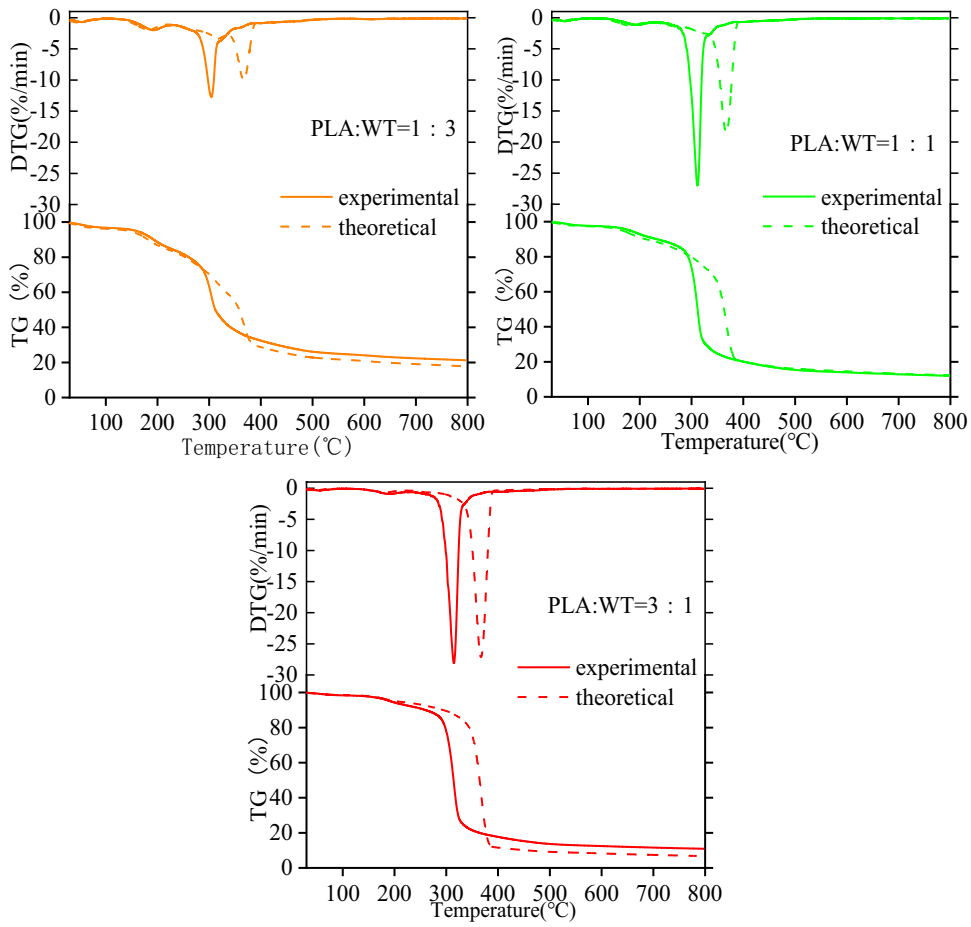

Fig. 3 The TG and DTG curve of PLA/WT at 10 °C/min heating rates

Table 1 Pyrolysis characteristic parameters of PLA in PLA/WT with different ratios

Sample	Temperature intervals (°C)		Weight loss (%)		T_{max} (°C)		DTG_{max} (%/min)	
	Experimental	Theoretical	Experimental	Theoretical	Experimental	Theoretical	Experimental	Theoretical
PLA	282.8–393.6	——	96.24	96.24	367.5	——	35.69	35.69
PLA/WT=1:3	230.8–315.5	328.1–390.0	36.08	31.80	303.8	366.4	12.69	10.06
PLA/WT=1:1	237.7–332.2	331.0–390.9	61.13	51.82	311.7	367.6	26.94	18.84
PLA/WT=3:1	231.3-330.6	333.7–393.4	66.73	67.86	314.1	372.5	28.01	26.61

in the DTG_{max}, which may be related to the small amount of WT. This indicated that the addition of WT could improve the thermal activity of PLA and exerted a positive synergistic effect during the co-pyrolysis process.

3.2 Pyrolysis kinetic analysis

Three model-free methods, FWO, DAEM, and Starink, were used to study the pyrolysis kinetics of PLA, WT, and PLA/WT blends. The fitting curve under the three methods was shown in Fig. 4. All three models showed a linear relationship between 1/T and lgβ (FWO), $\ln[\beta/T^2]$ (DAEM), and $\ln[\beta/T^{1.92}]$ (Starink) at different heating rates and the correlation coefficients (R^2) were higher than 0.95. The activation energy (E_a) of PLA, WT, and PLA/WT blends were calculated by three models at different conversion rates (α=0.2–0.8) were calculated. E_a represents the minimum energy required for a chemical reaction to occur higher and E_a indicates that more energy is required for a reaction to take place [31].

Tables 2, 3 and 4 showed the E_a and correlation coefficients at different conversion rates calculated through different kinetic methods. As shown in the tables, the correlation coefficients R^2 of all three methods at different conversion rates were greater than 0.95 and the difference in E_a calculated from different models was insignificant, which

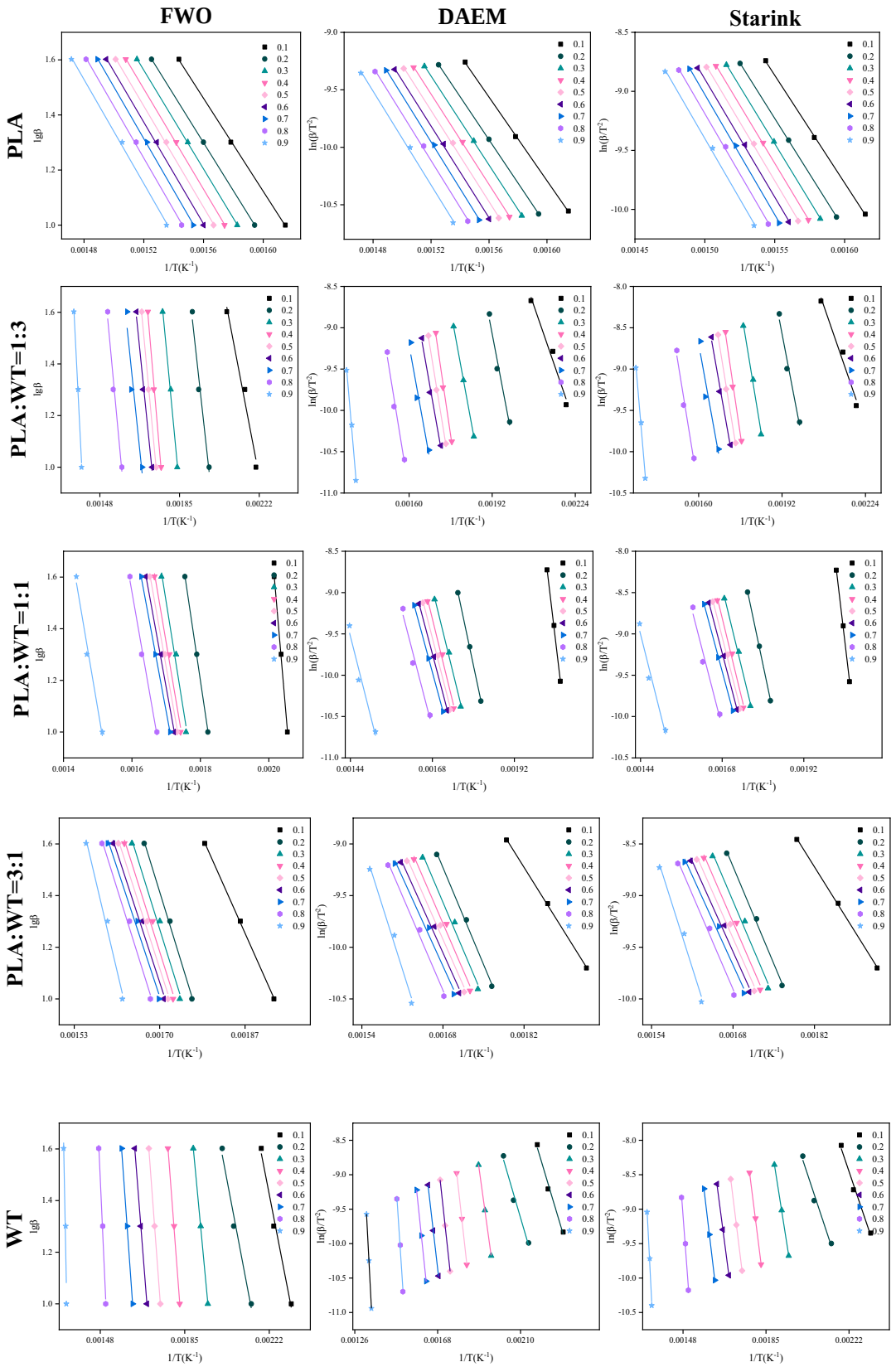

Fig. 4. Kinetic plots of PLA, WT, and PLA/WT blends according to the FWO, DAEM, and Starink methods

Table 2 E_a and R^2 of PLA, WT, and PLA/WT blends according to the FWO method

α	PLA		PLA:WT=1:3		PLA:WT =1:1		PLA:WT =3:1		WT	
	E_a	R^2	E_a	R^2	E_a	R^2	E_a	R^2	E_a	R^2
0.2	158.78	0.9999	137.86	0.9610	162.95	0.9992	115.04	0.9957	84.86	0.9720
0.3	163.21	0.9999	160.20	0.9913	151.10	0.9759	113.75	0.9823	171.69	0.9997
0.4	165.72	0.9997	178.00	0.9921	142.44	0.9858	112.06	0.9817	212.67	0.9984
0.5	167.07	0.9991	162.28	0.9959	136.71	0.9902	109.82	0.9815	217.27	0.9999
0.6	168.00	0.9990	149.46	0.9826	132.57	0.9955	107.95	0.9845	205.66	0.9996
0.7	170.86	0.9991	146.67	0.9692	129.85	0.9997	106.87	0.9819	226.55	0.9998
0.8	171.03	0.9984	163.40	0.9686	137.91	0.9880	112.92	0.9879	357.10	0.9849

Table 3 E_a and R^2 of PLA, WT, and PLA/WT blends according to the DAEM method

α	PLA		PLA:WT =1:3		PLA:WT =1:1		PLA:WT =3:1		WT	
	E_a	R^2	E_a	R^2	E_a	R^2	E_a	R^2	E_a	R^2
0.2	156.31	0.9999	136.45	0.9563	162.06	0.9991	111.28	0.9948	81.24	0.9668
0.3	160.89	0.9998	204.61	0.9979	140.06	0.9901	109.78	0.9787	171.88	0.9997
0.4	163.48	0.9996	177.60	0.9913	140.02	0.9836	107.93	0.9780	214.41	0.9982
0.5	164.85	0.9990	160.91	0.9954	133.93	0.9886	105.50	0.9775	218.80	0.9999
0.6	165.78	0.9988	147.31	0.9804	129.51	0.9947	103.48	0.9811	206.24	0.9995
0.7	168.73	0.9989	144.12	0.9519	126.59	0.9997	102.28	0.9778	227.83	0.9998
0.8	168.86	0.9981	161.10	0.9646	132.23	0.9449	108.55	0.9852	364.34	0.9839

Table 4 E_a and R^2 for PLA, WT, and PLA/WT blends according to the Starink method

α	PLA		PLA:WT =1:3		PLA:WT =1:1		PLA:WT =3:1		WT	
	E_a	R^2	E_a	R^2	E_a	R^2	E_a	R^2	E_a	R^2
0.2	155.49	0.9999	135.70	0.9565	161.14	0.9991	110.78	0.9948	80.91	0.9670
0.3	160.04	0.9998	158.35	0.9903	139.33	0.9901	109.30	0.9788	170.86	0.9997
0.4	162.61	0.9996	176.57	0.9914	139.30	0.9837	107.47	0.9781	213.08	0.9982
0.5	163.97	0.9990	160.02	0.9955	133.26	0.9887	105.06	0.9777	217.45	0.9999
0.6	164.90	0.9988	146.53	0.9805	128.88	0.9947	103.06	0.9812	205.00	0.9995
0.7	167.83	0.9989	143.38	0.9526	125.98	0.9997	101.87	0.9780	226.43	0.9998
0.8	167.96	0.9981	160.25	0.9648	131.58	0.9553	108.09	0.9853	361.90	0.9839

indicated the applicability of the models for studying the pyrolysis process of PLA, WT, and their blends. Figure 5 showed the comparison of kinetic parameter of E_a at different conversion rates. As can be seen, E_a of PLA pyrolysis increased slowly with increasing conversion. Taking the parameter calculated from FWO model as an example, the E_a increased from 158.78 to 171.03 KJ/mol when α varied from 0.2 to 0.8. This slow increasing trend may be related to the ordered molecular chains structure and higher purity of PLA. In addition, there was a difference in the energy required for the transesterification reaction and free radical reaction during the pyrolysis process of PLA, which may contribute to the increase of E_a [32]. The E_a for the pyrolysis of WT showed a trend of first increasing (α<0.4), then stabilizing (0.4<α<0.7) and finally rapidly increasing (α>0.7). This was due to the fact that the pyrolysis process of WT was gradually transformed from the release of volatile products to the cleavage of cellulose components at α<0.4. When the α increased from 0.4 to 0.7, the pyrolysis reactions were mainly related to the decomposition of lignocellulose components which possessed stable and complex polymer structure and high thermal stability. For α>0.7, the E_a significantly increased from 227 to 357 KJ/mol, which may be caused by the coverage of produced char with low reaction activity [33]. In addition, the E_a for WT were higher than that of PLA during the pyrolysis process of α>0.3. The average E_a for WT and PLA were 210.83 and 166.38 KJ/mol, respectively.

Furthermore, as for the co-pyrolysis of PLA/WT blends, the average E_a for PLA/WT=1:3 was 156.84 KJ/mol, the average E_a of PLA/WT=1:1 was 141.93 KJ/mol and the average E_a of PLA/WT=3:1 was 111.20 KJ/mol. The E_a of PLA/WT blends was generally lower than that of solo PLA and WT during the pyrolysis process. Different mixture ratios of

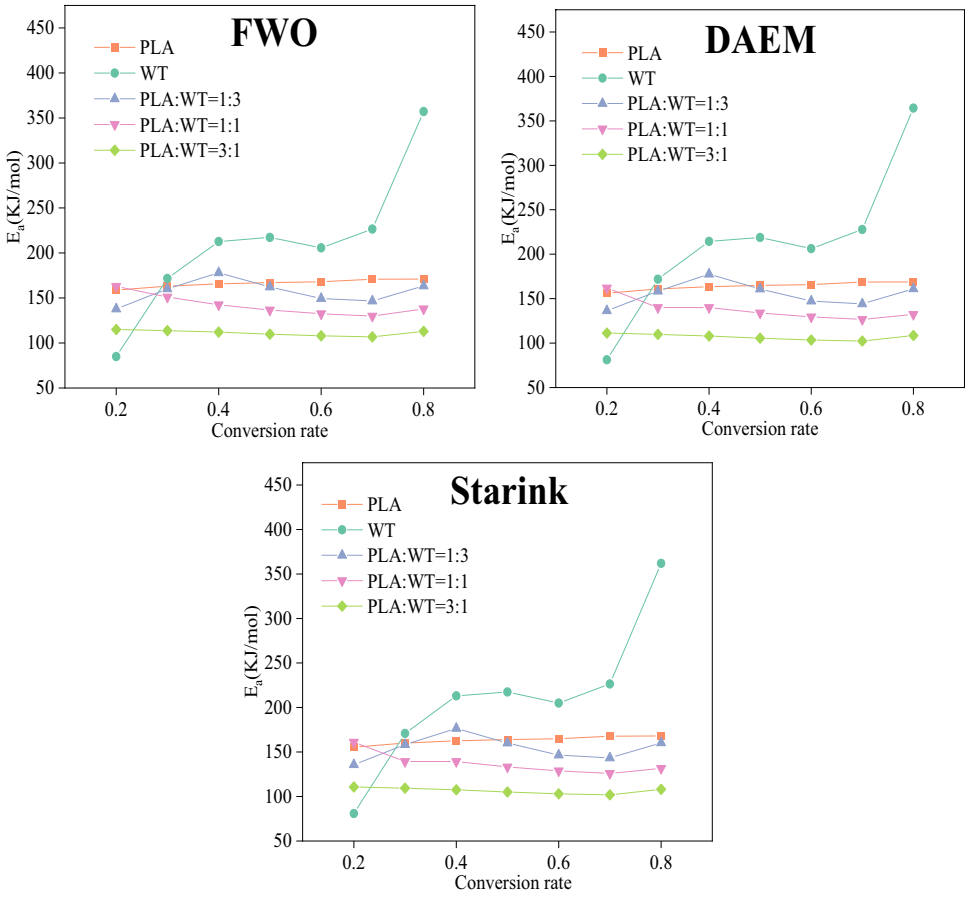

Fig. 5 Comparison of kinetic parameters at different conversion rates

WT showed different degrees of reduction in E_a. In particular, the greatest reduction in E_a was achieved when the addition ratio of WT was 25%. This indicated that the appropriate proportion of WT addition could reduce the energy required for the pyrolysis of PLA. The reduced E_a of the mixture indicated that a synergistic effect was existed during the co-pyrolysis process of PLA/WT. This was probably because the free radicals generated by WT pyrolysis could promote free radical reactions in PLA pyrolysis [34, 35].

The thermodynamic parameters such as enthalpy (ΔH), Gibbs free energy (ΔG), and Entropy (ΔS) were calculated from the E_a, by using the FWO method and analyzing data with a heating rate of 10 °C/min. The results of the thermodynamic parameters at different α were shown in Fig. 6. ΔH represents the total energy consumed for the pyrolysis of reactant into various pyrolytic products [33], and in this study it represents the total energy used for the co-pyrolysis of PLA/WT. The difference between E_a and ΔH is referred to as activation energy barrier, which is directly proportional to the difficulty of pyrolysis reaction. According to calculation, activation energy barriers for different PLA/WT blends were around 5 KJ/mol which was relatively lower than that of PLA (15 KJ/mol) indicating the addition of WT was beneficial for the PLA pyrolysis. ΔG reflects the changes in total energy of a system and higher values indicates that it is less favorable for a chemical process to occur [36]. As seen from Fig. 6, Gibbs free energies of different PLA/WT blends were ranged from 146.39 to 151.96 KJ/mol, which was significantly lower than that of PLA (164. 53–164.92 KJ/mol). This reduced ΔG suggested that the synergistic effect promoted the co-pyrolysis process. The entropy change (ΔS) during pyrolysis reflected the degree of disorderly change of pyrolysis substances and products [37]. The larger fluctuation of ΔS value indicates the more unstable reactivity of different pseudo-components in the pyrolysis process. As shown in the figure, the ΔS of PLA alone was the most stable, and the addition of WT greatly enhanced the fluctuation of ΔS. This also indicated that the addition of WT increased the reactivity of PLA.

3.3 TG-FTIR analysis

TG-FTIR was used to characterize the synergistic effect of PLA/WT blends during the pyrolysis. The 3D infrared spectra of blends with different proportions of PLA and WT were shown in Fig. 7. The functional groups represented by each peak in the infrared spectrum were shown in Table 5 [38]. According to Beer-Lambert law, the absorbance of pyrolysis

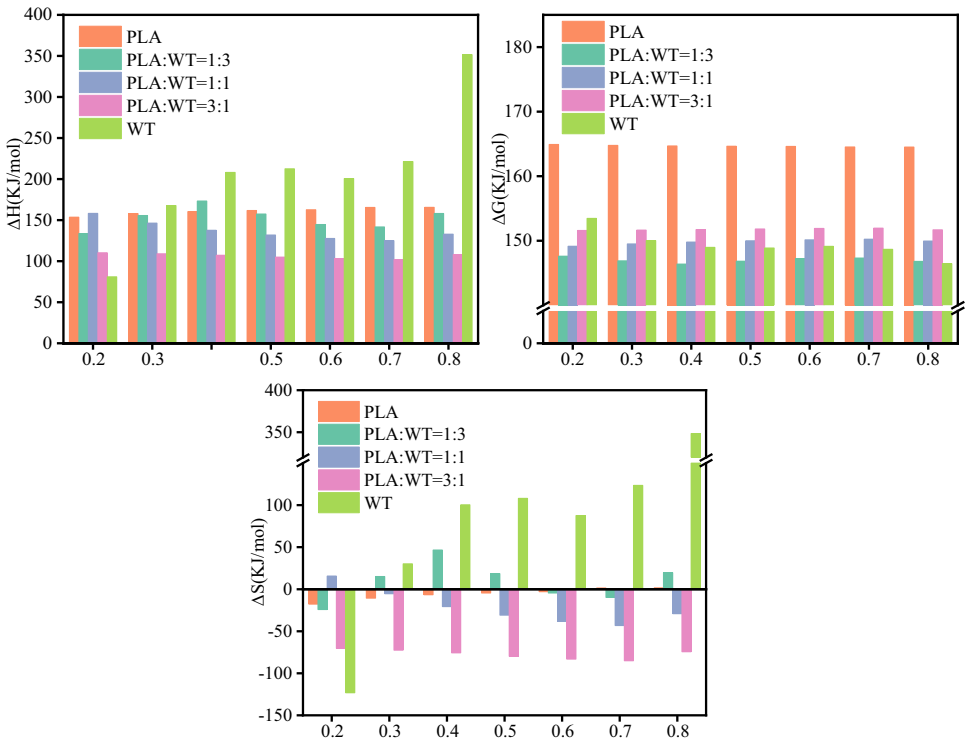

Fig. 6 Thermodynamic parameters of ΔH, ΔG, ΔS

products is proportional to its concentration. Among the products generated by PLA pyrolysis, the absorption band at 1650–1900 cm^{-1} exhibited the highest absorbance, which corresponded to the stretching vibration of C=O and represented the generation of ester products such as lactide. Meanwhile, the stretching vibration at 1980–2240 cm^{-1} represented the production of CO, and the stretching vibration at 2640–2800 cm^{-1} represented the production of aldehyde, both CO and aldehyde were specific products of transesterification reaction; the stretching vibration at 2240–2400 cm^{-1} represented the production of CO_2, which was a specific product of free radical reaction [39]. The pyrolysis products of WT were mainly consisted of large amounts of CO_2 and small amounts of ketones, acids, esters (1650–1900 cm^{-1}), and CH_4 (2640–3100 cm^{-1}).

In addition, to investigate the conversion between transesterification reactions and free radical reactions during PLA pyrolysis, we focused on the release of their characteristic products (aldehyde, CO, CO_2). Figure 8 exhibited the released pyrolytic gaseous of C=O, C-O, and O-C-H groups as reflected by infrared peaks changing with temperature. It could be seen from the Fig. 8 that the maximum infrared absorption peak of PLA was between 310–380 °C, and that of PLA/WT blends was between 260 and 330 °C, which proved that co-pyrolysis of PLA/WT reduced the reaction temperature, and the temperature range for product generation was more concentrated. At the same time, it could be seen that the peak shape of the ester bond (1650–1900 cm^{-1}) changed most significantly compared to solo PLA, indicating that co-pyrolysis promoted the generation of products containing the ester bond. From 3D spectrum it could be seen that as for the sample of PLA/WT=1:1, the peak absorption of ester bond was higher than that of other blends. At same time, the peak for CO was basically disappeared, and the peak of O-C-H (aldehyde) was greatly reduced as for the PLA/WT blends. It was known that CO and aldehyde were specific products for transesterification reaction, indicating the synergistic effect was reflected by the suppression of transesterification reaction and promotion of free radical reaction pathway during the co-pyrolysis process.

3.4 GC–MS analysis of gaseous product

The total ion chromatogram of the pyrolysis products of individual PLA, WT and WT/PLA blends was shown in Fig. 9. The main products generated during pyrolysis process were shown in Table 4. As could be seen from Fig. 9, the characteristic pyrolysis products of PLA/WT blends, such as CO_2, acetaldehyde, meso-lactide, and D, L-lactide were detected. These categories of products were also monitored by TG-FTIR as mentioned above. Acetaldehyde and CO were special products of the transesterification reaction, while meso-lactide and CO_2 were special products of free radical reaction [40]. The mechanism of the pyrolysis reaction could be inferred from the difference in the type and content of the pyrolysis products. In order to further investigate the effect of WT addition on the yield of specific products during co-pyrolysis, the theoretical percentage

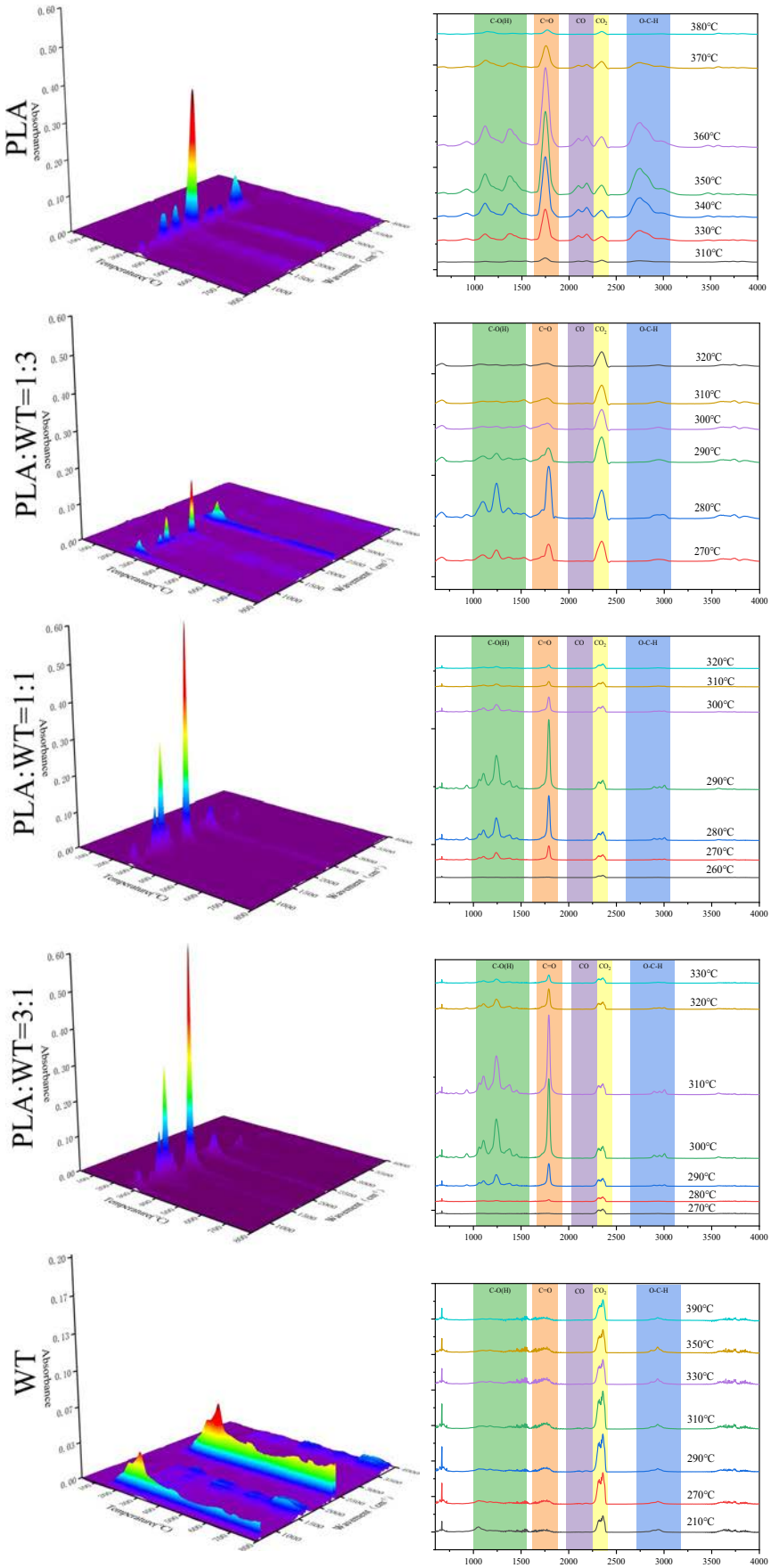

Fig. 7 3D-FTIR spectra of products during pyrolysis of PLA, WT, PLA/WT, and PLA/WT blends; FTIR spectra of products during pyrolysis at different temperatures of PLA, WT, PLA/WT, and PLA/WT blends

Table 5 The functional groups represented by each peak in the FTIR spectrum

Wavenumber (cm^{-1})	Vibration	Functional group	Product
4000–3500	Stretching	-OH	H_2O/Phenols/Alcohols
3100–2640	Stretching	C-H	CH_4
2800–2640	Stretching	O-C-H	Aldehyde
2400–2240	Stretching	C=O	CO_2
2240–1980	Stretching	C-O	CO
1900–1650	Stretching	C=O	ketones/acids/esters
1400–1000	Stretching	C-O(H)	Alcohols/phenols/ethers
680–660	Bending	C=O	CO_2

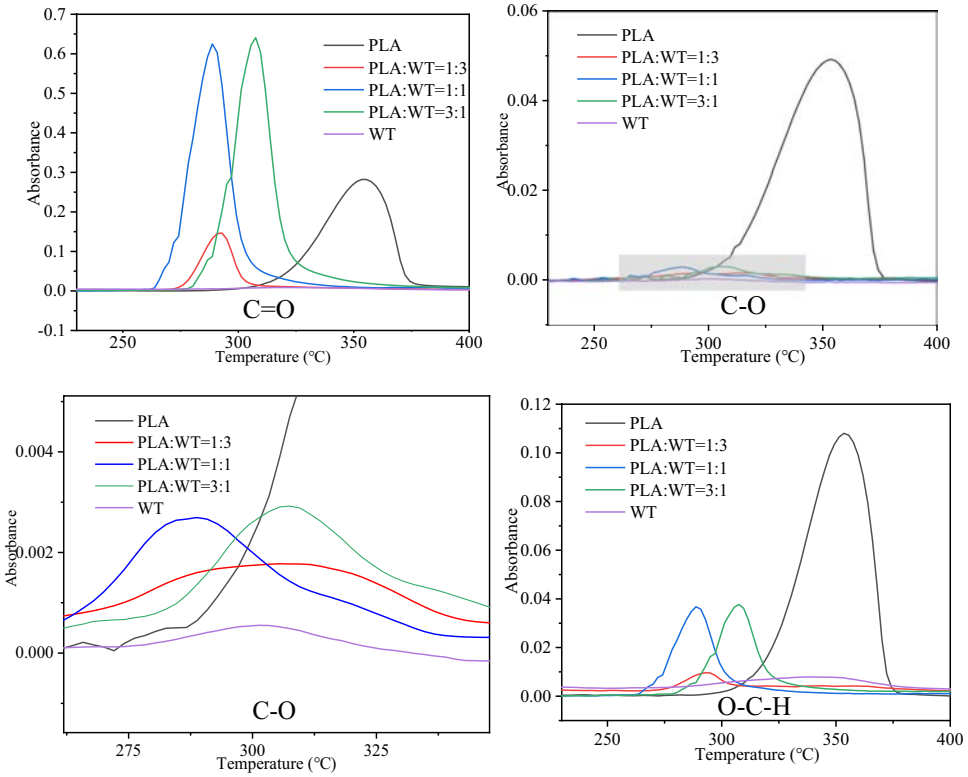

Fig. 8 The infrared peaks of C=O, C-O, O-C-H groups changing with temperature

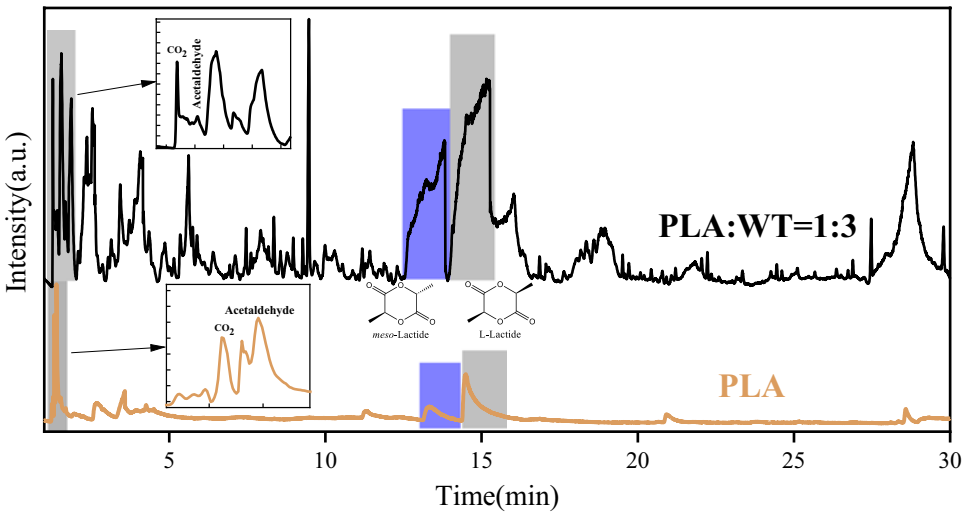

Fig. 9 The ion chromatogram of PLA and PLA/WT products after pyrolysis

Table 6 The main products generated during pyrolysis by Py-GC/MS

Compound	Peak area(%)							
	PLA	PLA/WT=1/3		PLA/WT=1/1		PLA/WT=3/1		WT
	Percentage	Percentage	Theoretical Percentage	Percentage	Theoretical Percentage	Percentage	Theoretical Percentage	Percentage
Carbon dioxide	2.242	0.434	1.02	0.199	1.428	0.419	1.835	0.613
Acetaldehyde	6.425	0.256	1.924	0.114	3.424	0.255	4.925	0.423
meso-Lactide	7.344	7.606	1.836	25.178	3.672	10.581	5.508	0
D,L-Lactide	21.665	5.751	5.416	18.505	10.833	13.258	16.249	0

content of each product was calculated by weighted average of the content percentage of pyrolysis product for solo PLA and WT. The theoretical percentage content of the products can be expressed as follows [41]:

$$P_{blend}(\%) = \omega_{PLA}P_{PLA}(\%) + \omega_{WT}P_{WT}(\%) \quad (14)$$

In the above equation, P_{blend} is the theoretical percentage content of a certain product after PLA/WT co-pyrolysis, ω is the proportion of samples in PLA/WT blends, and P_{PLA} and P_{WT} are the percentage contents of a certain product after pyrolysis for solo PLA or WT, respectively. The calculation results were shown in Table 6.

During the co-pyrolysis of PLA/WT, the actual percentage content of CO_2 and acetaldehyde were between 0.199–0.434% and 0.114–0.256%, respectively, which were far lower than their theoretical percentage contents. Meanwhile, the actual content of lactide was higher than that of theoretical content. This indicated that synergistic effect exerted an obvious inhibitory effect on the formation of acetaldehyde. The variation in

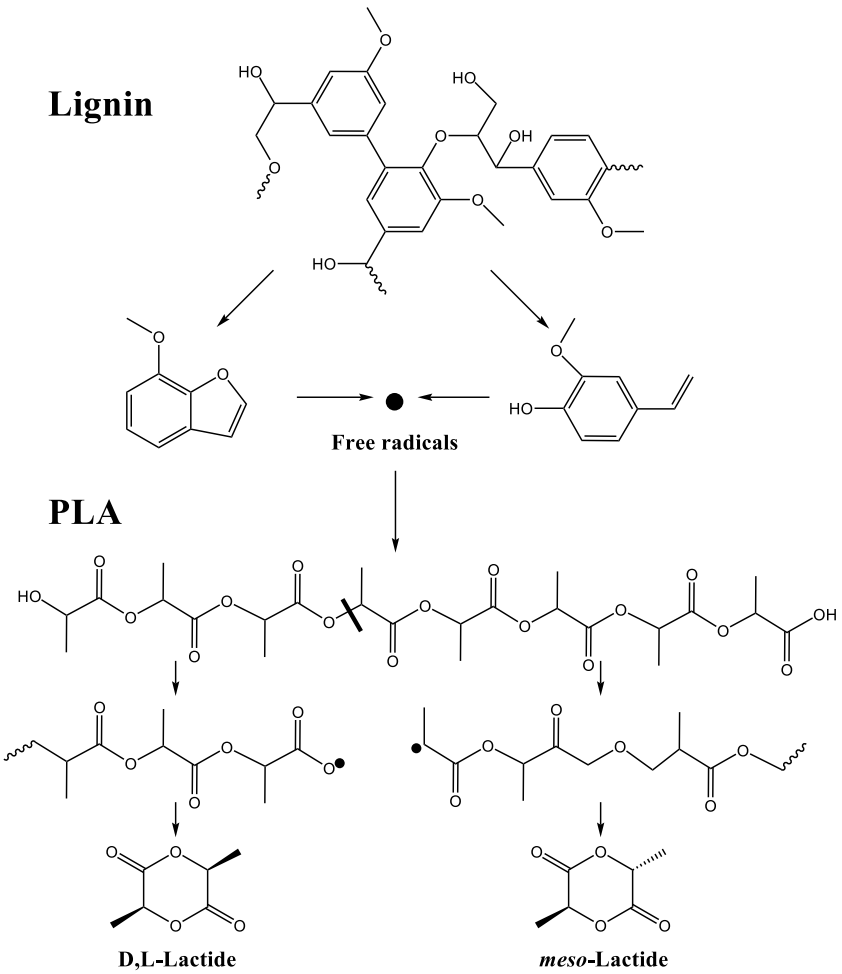

Fig. 10 The possible promotion mechanism during co-pyrolysis of lignin and PLA

the content of acetaldehyde suggested that the co-pyrolysis of PLA/WT changed the process of generating lactide from an esterification reaction to a free radical reaction pathway [17]. According to previous reports, End-capped PLA chains with free radicals combined with hydrogen ions from WT to form -O=C-OH structure which inhibited rearrangement of PLA chains, resulting in reduced generation of CO_2 [42] . Meanwhile, under different proportions mixed ratio, the actual percentage content of meso-Lactide was also higher than its theoretical percentage content in varied degrees. This indicated that WT can promote the free radical reaction of PLA in some extent. In the free radical reaction pathway, the PLA chains was broken into analkyl-oxygen or acly-oxygen bonds and combined with the free radicals produced during the pyrolysis of WT, which further undergo stereo isomerization and eventually promote the production of meso-lactide (Fig. 10). As for the sample of PLA/WT=1:1, the percentage content of meso-Lactide was 6.9 times higher than its theoretical value, while the content of total Lactide was 3 times higher than its theoretical value. The promoting effect as for PLA/WT=1:1 was obvious higher than that of other mixtures ratios, indicating an optimal addition ratio of WT was existed for the co-pyrolysis of blends.

The pyrolytic products trapped by the Cambridge filter were further analyzed through GC–MS. The results were shown in Table 7. The pyrolysis products of PLA were mainly meso-lactide (483.4 ug/g), D, L-lactide (1199.3 ug/g), propanoic acid (24.3 ug/g), 2-propanoic acid (64.1 ug/g), acetaldehyde (7.5 ug/g), and other substances generated through transesterification and free radical reaction as well as secondary cracking process. The pyrolysis products of WT mainly included nicotine, ketones, and phenols products that produced during the heating and pyrolysis process. After mixing PLA with WT, it could be observed that a significant increase in the production of meso lactide and D, L-lactide, indicating the synergistic effect existed during the pyrolysis process of PLA and WT.

Moreover, the increase in the content of meso-lactide was greater than that of D, L-lactide. For example, as for the sample of PLA:WT=1:1, the yield of meso-lactide increased by 2.2 times, the yield of D, L-lactide increased by 1.2 times as compared with that of PLA alone, which was consistent with the results of Py-GC/MS. It should be noted that sample of PLA:WT=3:1 here exhibited the most significant synergistic effect, which was different from the results of Py-GC/MS. This phenomenon may be related to

Table 7 The main products generated during pyrolysis by Infrared heated tubular furnace combined with GC/MS analysis

No.	Compounds	Formula	Content (ug/g)				
			PLA	25PLA 75WT	50PLA 50WT	75PLA 25WT	WT
1	3-Hexanone	$C_6H_{12}O$	4.6	81.5	121.2	47.7	
2	Propanoic acid	$C_3H_6O_2$	24.3	126.3	169.3	225.2	103.7
3	2-Propenoic acid	$C_3H_4O_2$	64.1	117.9	163.5	519.7	
4	Acetaldehyde	C_2H_4O	7.5				
5	2-Cyclopenten-1-one	C_5H_6O		82.3	109.3	90.5	77.6
6	2-Furanmethanol	$C_5H_6O_2$		93.4	54.7	15.8	135.5
7	1-(Acetyloxy)-2-propanone	$C_5H_8O_3$	137.1	213.9	461.6	707.1	79.6
8	2-Methyl-2-cyclopenten-1-one	C_6H_8O		302.1	229.4	58.4	368.9
9	3-Methyl-2-cyclopenten-1-one	C_6H_8O		156.3	83.6	65.3	228.6
10	Phenol	C_6H_6O		386.7	242.6	118.2	594.8
11	2-Methyl-phenol	C_7H_8O		183.6	100.6	89.5	300.4
12	Acetophenone	C_8H_8O		23.8	15.4	11.9	50.4
13	2-Methoxy-phenol	$C_7H_8O_2$		83.5	42.6	27.7	152.5
14	2,4-Dimethyl-Phenol	$C_8H_{10}O$		61.4	21.3	9.9	110.5
15	3-Ethyl-2-hydroxy-2-cyclopenten-1-one	$C_7H_{10}O_2$		103.1	83.7	29.5	128.1
16	Meso-lactide	$C_6H_8O_4$	483.4	914.2	1526.2	9062.8	
17	2,5-Dimethyl-phenol	$C_8H_{10}O$		230.4	179.2	125.5	270.5
18	D,L-lactide	$C_6H_8O_4$	1199.3	1483.4	2635.2	12573.7	
19	2,6-Dimethyl-phenol	$C_8H_{10}O$		75.8	57.1	9.9	97.8
20	4-Ethyl-3-methyl-phenol	$C_9H_{12}O$		68.1	43.6	34.7	80.7
21	2-Methoxy-4-vinylphenol	$C_9H_{10}O_2$		28.3	16.8	13.4	49.8
22	Nicotine	$C_{10}H_{14}N_2$		2461.8	810.4	278.2	3268.4
23	2,2'-Methylenebis[6-(1,1-dimethylethyl)-4-methyl-phenol	$C_{23}H_{32}O_2$	15.4	38.4	102.1	64.4	

the heating rate and contact state between melted PLA and WT in the these two pyrolysis experimental conditions [43].

4 Conclusion

In conclusion, this study investigated the effects of synergistic interaction on pyrolysis characteristics and products during the co-pyrolysis of PLA and WT in HTPs waste through thermogravimetric analysis, TG-FTIR and Py-GC/MS. The results showed that the addition of WT could improve the thermal activity of PLA and enhance the reaction. The synergistic effect of PLA/WT co-pyrolysis effectively reduced the activation energy required for pyrolysis. The impact of 25%wt of WT addition was most significant, the activation energy of co-pyrolysis reaction decreased by 33.2% compared to that of solo PLA. Meanwhile, the synergistic effect can reduce the activation energy barrier and Gibbs free energy of the reaction. It indicating that the synergistic effect can effectively reduce the input of external power and save energy. The TG-FTIR results showed that the addition of WT promoted free radical reactions during the co-pyrolysis process of PLA, significantly increasing the yield of ester products. Py-GC/MS results indicated that for PLA/WT=1:1, the yield of lactide increased 3 times, infrared heated tubular furnace-GC/MS results indicated that for PLA/WT=3:1, the yield of lactide increased 12 times, showing that synergistic effect had a significant impact. Also, it showed that pyrolysis and stacking methods had an effect on co-pyrolysis. In summary, the co-pyrolysis could effectively tap into residual value from discarded PLA and WT in resource recovery field, solve potential environmental pollution problems, and have potential for material recovery.

Author contributions All authors contributed to the study conception and design. The summary is as follows: Conceptualization: Junsong Zhang and Miao Liang. Material preparation: Yongjie Zheng and Man Su. Methodology: Yifei Xie and Ruili Li. Formal analysis and investigation: Haiyang Pan, Yuanyang Zhu, Miao Liang, and Xi Jiang. Writing—original draft preparation: Haiyang Pan and Miao Liang. Writing—review and editing: Haibo Zhu, Xi Jiang, Ruili Li, and Miao Liang. Funding acquisition: Haibo Zhu and Junsong Zhang. Supervision: Miao Liang and Junsong Zhang. All authors read and approved the final manuscript.

Funding This work was supported by the Research Foundation (H202232) of Nantong Cigarette Filter Co., Ltd.

Data availability The datasets generated during and/or analyzed during the current study are available from the corresponding author on reasonable request.

Declarations

Ethical approval NA.

Competing interests The authors declare no competing financial interest.

References

1. Kim Y-H, An Y-J, Shin J-W (2020) Carbonyl compounds con-taining formaldehyde produced from the heated mouthpiece of tobacco sticks for heated tobacco products. Molecules 25:5612. https://doi.org/10.3390/molecules25235612
2. Chen J, He X, Zhang X, Chen Y, Zhao L, Su J, Qu S, Ji X, Wang T, Li Z, He C, Zeng E, Jin Y, Lin Z, Zou C (2021) The applicability of different tobacco types to heated tobacco products. Ind Crops and Prod 168:113579. https://doi.org/10.1016/j.indcrop.2021.113579
3. Simonavicius E, McNeill A, Shahab L, Brose LS (2019) Heat-not-burn tobacco products: a systematic literature review. Tob Control 28:582–594. https://doi.org/10.1136/tobaccocontrol-2018-054419
4. Zhao L, Shang SZ, Tian YF, Gao YL, Song ZB, Peng LJ, Li ZL, Wang BW (2023) Integrative analysis of sensory evaluation and non-targeted metabolomics to unravel tobacco leaf metabolites associated with sensory quality of heated tobacco. Front Plant Sci 14:1123100. https://doi.org/10.3389/fpls.2023.1123100
5. Choi Y, Jeong S, Park Y-K, Kim H, Lim S-J, Woo G-J, Pyo S, Siddiqui MZ, Kim Y-M (2021) Chemical feedstock recovery via the pyrolysis of electronically heated tobacco wastes. Sustainability 13(22):12856. https://doi.org/10.3390/su132212856
6. Sun C, Wei S, Tan H, Huang Y, Zhang Y (2022) Progress in upcycling polylactic acid waste as an alternative carbon source: a review. Chem Eng J 446:136881. https://doi.org/10.1016/j.cej.2022.136881
7. Chen Y, Chen M, Zhang W, Zhang S, Su X, Zhao T, Chen Y, Su X, Zeng J, Cao J, Liu Z, Zhong L, Wang G (2023) Large-scale isolation of scopoletin from Nicotiana tabacum. Biomass Convers Biorefin. https://doi.org/10.1007/s13399-023-03778-w
8. Zhang J, Zou H, Liu J, Evrendilek F, Xie W, He Y, Buyukada M (2021) Comparative (co-)pyrolytic performances and by-products of textile dyeing sludge and cattle manure: deeper insights from Py-GC/MS, TG-FTIR, 2D-COS and PCA analyses. J Hazard Mater 401:123276. https://doi.org/10.1016/j.jhazmat.2020.123276
9. Wijana S, Atikah H, Kartikaningrum W, Pranowo D, Setyawan HY (2023) An experimental study of application of activated carbon from nipa fruit waste on herbal drinks. Sustainable Environ 9:2173024. https://doi.org/10.1080/27658511.2023.2173024
10. Alabi AO, Sambo AS (2023) Comparative bio-energy potential of de-oiled coconut pulp and coconut shell: insights from physico-chemical characterization, pyrolysis kinetics and thermodynamic studies. Fuel Process Technol 243:107658. https://doi.org/10.1016/j.fuproc.2023.107658
11. Chien YC, Liang CJ, Yang SH (2011) Exploratory study on the pyrolysis and PAH emissions of polylactic acid. Atmos Environ 45:123–127. https://doi.org/10.1016/j.atmosenv.2010.09.035
12. Zhang F, Sun Y, Li J, Su H, Zhu Z, Yan B, Cheng Z, Chen G (2022) Pyrolysis of 3D printed polylactic acid waste: a kinetic study via TG-FTIR/GC-MS analysis. J Anal Appl Pyrolysis 166:105631. https://doi.org/10.1016/j.jaap.2022.105631
13. Yildiz Z, Ceylan S (2019) Pyrolysis of tobacco factory waste biomass. J Therm Anal Calorim 136:783–794. https://doi.org/10.1007/s10973-018-7630-z
14. Xia Q, Yan B, Wang H, Xu J, Zhang S, Zhou G, Hu A, Jiang J, Xu S, Wang J, Chen W (2020) Production of bio-oils enriched with aroma compounds from tobacco waste fast pyrolysis in a fluidized bed reactor. Biomass Convers Biorefin 11:1611–1619. https://doi.org/10.1007/s13399-019-00578-z

15. Sun C, Li C, Tan H, Zhang Y (2019) Synergistic effects of wood fiber and polylactic acid during co-pyrolysis using TG-FTIR-MS and Py-GC/MS. Energy Convers Manag 202:112212. https://doi.org/10.1016/j.enconman.2019.112212
16. Aoyagi Y, Yamashita K, Doi Y (2002) Thermal degradation of poly[(R)-3-hydroxybutyrate], poly[ε-caprolactone], and poly[(S)-lactide]. Polym Degrad Stab 76(1):53–59. https:// doi. org/ 10. 1016/ S0141- 3910(01) 00265-8
17. Sobek S, Werle S (2020) Isoconversional determination of the apparent reaction models governing pyrolysis of wood, straw and sewage sludge, with an approach to rate modelling. Renew Energ 161:972–987. https://doi.org/10.1016/j.renene.2020.07.112
18. Kopinke FD, Remmler M, Mackenzie K, Möder M, Wachsen O (1996) Thermal decomposition of biodegradable polyesters—II. Poly(lactic acid). Polym Degrad Stab 53(3):329–342
19. Sun C, Chen X, Zheng D, Yao W, Tan H, Zhang Y, Liu S (2021) Exploring the synergetic effects of the major components of bio-mass additives in the pyrolysis of polylactic acid. Green Chem 23:9014–9023. https://doi.org/10.1039/d1gc03002g
20. Lu P, Huang Q, Bourtsalas AC, Chi Y, Yan J (2018) Synergistic effects on char and oil produced by the co-pyrolysis of pine wood, polyethylene and polyvinyl chloride. Fuel 230:359–367. https://doi.org/10.1016/j.fuel.2018.05.072
21. Kopinke FD, Mackenzie K (1997) Mechanistic aspects of the ther-mal degradation of poly(lactic acid) and poly(β-hydroxybutyric acid). J Anal Appl Pyrolysis 40:43–53
22. Liang M, Zhang K, Lei P, Wang B, Shu CM, Li B (2020) Fuel properties and combustion kinetics of hydrochar derived from co-hydrothermal carbonization of tobacco residues and graphene oxide. Biomass Convers Biorefin 10:189–201. https://doi.org/10.1007/s13399-019-00408-2
23. Trinh VT, Lee B-H, Jeong T-Y, Jeon C-H (2023) Pyrolysis of different rank fuels: characteristics and kinetic parameter study using nonlinear optimization and artificial neural network. J Therm Anal Calorim. https://doi.org/10.1007/s10973-023-12084-6
24. Uzun ZY (2023) Investigation of fuel properties of hydrochars obtained from pomegranate peel: characterization and combustion kinetic. Biomass Convers Biorefin. https://doi.org/10.1007/s13399-023-03840-7
25. Manuel Rêgo Silva J, de Morais M, Araújo A, da Costa P, Evangelista J, Ribeiro da Silva D, Duarte Gondim A, Souza de Araujo A (2023) Evaluation of the kinetic and thermodynamic parameters in catalytic pyrolysis process of sunflower oil using Al-MCM-41 and zeolite H-ZSM-5. Fuel 333:126225. https://doi.org/10.1016/j.fuel.2022.126225
26. Alhulaybi Z, Dubdub I, Al-Yaari M, Almithn A, Al-Naim AF, Aljanubi H (2023) Pyrolysis kinetic study of polylactic acid. Polymer 15(1):12. https://doi.org/10.3390/polym15010012
27. Wu J, Chen Z, Wang J, Wang Y, Jiang J, Xiao W, Xia Q, Zhang J, Zhou G, Zhang J, Liang M (2022) Effect of glycerol addition on the pyrolysis characteristics and pyrolytic product distribution of cigar tobacco. Biomass Convers Biorefin. https://doi.org/10.1007/s13399-022-03175-9
28. Zhang XD, Xu M, Sun RF, Sun L (2006) Study on biomass pyrol-ysis kinetics. J Eng Gas Turbines Power 128:493–496. https://doi.org/10.1115/1.2135816
29. Melkior T, Jacob S, Gerbaud G, Hediger S, Le Pape L, Bonnefois L, Bardet M (2012) NMR analysis of the transformation of wood constituents by torrefaction. Fuel 92:271–280. https://doi.org/10.1016/j.fuel.2011.06.042
30. Dai Y, Xu J, Zhu L, Jiang J, Zhou Y, Zhou G (2021) Mechanism study on the effect of glycerol addition on tobacco pyrolysis. J Anal Appl Pyrolysis 157:105183. https://doi.org/10.1016/j.jaap.2021.105183
31. Liao YF, Ma XQ (2010) Thermogravimetric analysis of the co-combustion of coal and paper mill sludge. Applied Energy 87:3526–3532. https://doi.org/10.1016/j.apenergy.2010.05.008
32. Cai JM, Liu RH (2008) Numerical analysis of new distributed activation energy model for the representation of biomass pyrolysis kinetics. J Energy Inst 81:149–152. https://doi.org/10.1179/174602208X330266
33. Sun C, Yang Z, Zheng Z, Li W, Tan H, Huang Y, Zhang Y (2023) Exploring how lignin promoting the co-pyrolysis with polylactic acid: artificial neural network modeling, kinetic analysis and product distribution. Sustainable Mater Technol 35:e00549. https://doi.org/10.1016/j.susmat.2022.e00549
34. Sivalingam G, Madras G (2004) Thermal degradation of binary physical mixtures and copolymers of poly(epsilon-caprolactone), poly(D, L-lactide), poly(glycolide). Polym Degrad Stab 84:393–398. https://doi.org/10.1016/j.polymdegradstab.2003.12.008
35. Navarro MV, López JM, Veses A, Callén MS, García T (2018) Kinetic study for the co-pyrolysis of lignocellulosic biomass and plastics using the distributed activation energy model. Energy 165:731–742. https://doi.org/10.1016/j.energy.2018.09.133
36. Mao J, Xiao C, Gong D, Zhu J, Qian J (2023) Study on mechanism of cellulose hydrolysis during alkali thermal pretreatment of lignocellulose by density functional theory. Biomass Bioenergy 172:106754. https://doi.org/10.1016/j.biombioe.2023.106754
37. Kaur R, Gera P, Jha MK, Bhaskar T (2018) Pyrolysis kinetics and thermodynamic parameters of castor (Ricinus communis) residue using thermogravimetric analysis. Bioresour Technol 250:422–428. https://doi.org/10.1016/j.biortech.2017.11.077
38. Alhumade H, Alayed OS, Iqbal MW, Shahid A, Iqbal T, Ahmad MS, Elkamel A, Al-Turki Y, Mehmood MA, Ashraf GA (2023) Exploration of the bioenergy potential of Dactyloctenium aegyptium through pyrolysis, kinetics, and thermodynamic parameters to produce clean fuels and biochemicals. Fuel 341:127663. https://doi.org/10.1016/j.fuel.2023.127663
39. Sun C, Li W, Chen X, Li C, Tan H, Zhang Y (2021) Synergistic interactions for saving energy and promoting the co-pyrolysis of polylactic acid and wood flour. Renew Energy 171:254–265. https://doi.org/10.1016/j.renene.2021.02.099
40. Shao Z, Kumagai S, Kameda T, Saito Y, Yoshioka T (2023) Effects of heating rate and temperature on product distribution of poly-lactic acid and poly-3-hydroxybutyrate-co-3-hydroxyhexanoate. J Mater Cycles Waste Manage 25:650–661. https://doi.org/10.1007/s10163-022-01573-9
41. Omura M, Tsukegi T, Shirai Y, Nishida H, Endo T (2006) Thermal degradation behavior of poly(lactic acid) in a blend with polyethylene. Ind Eng Chem Res 45:2949–2953. https://doi.org/10.1021/ie051446x
42. Khodaparasti MS, Khorasani R, Tavakoli O, Khodadadi AA (2023) Optimal Co-pyrolysis of municipal sewage sludge and microalgae Chlorella Vulgaris: products characterization, synergistic effects, mechanism, and reaction pathways. J Cleaner Prod 390:135991. https://doi.org/10.1016/j.jclepro.2023.135991
43. Fan Y, Liu C, Kong X, Han Y, Lei M, Xiao R (2022) A new perspective on polyethylene-promoted lignin pyrolysis with mass transfer and radical explanation. Green Energy Environ 7:1318–1326. https://doi.org/10.1016/j.gee.2021.02.004